Front. Phys., 2012, 7(4): 429–434
DOI 10.1007/s11467-011-0201-4

RESEARCH ARTICLE

Electronic structure of YMn_2O_5 studied by EELS and first-principles calculations

Zhen Chen, Rui-Juan Xiao, Chao Ma, Yuan-Bin Qin, Hong-Long Shi, Zhi-Wei Wang, Yuan-Jun Song, Zhen Wang, Huan-Fang Tian, Huai-Xin Yang, Jian-Qi Li†

Beijing National Laboratory for Condensed Matter Physics, Institute of Physics, Chinese Academy of Sciences, Beijing 100190, China

E-mail: †*ljq@aphy.iphy.ac.cn*

Received May 23, 2011; accepted July 5, 2011

The electronic structure of multiferroic YMn_2O_5 material has been studied by use of the generalized gradient approximation (GGA). The results demonstrate that the oxygen 2p and manganese 3d orbitals are strongly hybridized. Considering the on-site Coulomb interaction U, we performed the GGA+U calculations for $0 < U \leqslant 8$ eV, and it is found that the increase of U could enlarge the band gap and, on the other hand, weaken the Mn–O hybridization. The experimental measurements of the electron energy-loss spectrometry (EELS) exhibit a rich variety of structural features in both O–K edge and Mn–L edges. A theoretical and experimental analysis on the O–K edge suggests that the on-site Coulomb interaction (U) in YMn_2O_5 could be less than 4 eV. Certain electronic structural features of $LaMn_2O_5$ have been discussed in comparison with those of YMn_2O_5.

Keywords YMn_2O_5, multiferroics, electron energy-loss spectra, electronic structure, GGA+U

PACS numbers 75.85.+t, 79.20.Uv, 71.15.Mb

1 Introduction

Multiferroics with several order parameters in single phase compounds have been a subject of major scientific interest for many years. These materials exhibiting coupling between electrical polarization, spontaneous magnetization and strain have potential technological applications [1–3]. However, multiferroic materials, as reported in previous literatures, often show a relatively weak coupling. Recently, giant magnetoelectric (ME) effects have been observed in a class of mixed-valent manganese oxides, $REMn_2O_5$ (RE = Y, Tb, Dy, *et al.*) [4], in which the remarkable ME coupling and the magnetic transitions have been extensively discussed [3, 5, 6]. The $REMn_2O_5$ compounds have complex magnetic structures at low temperatures associated with the commensurate or incommensurate antiferromagnetic (AFM) phase depending on the rare-earth elements [7, 8]. Theoretical investigations on the microscopic mechanism of giant ME effects also obtained a variety of interesting results as regard to these manganese oxides. A collinear AFM structure with the propagation vector $\boldsymbol{k} = (0.5, 0, 0)$ is a good approximation for the noncollinear magnetic ordering of Mn atoms, as recognized from good agreements between certain experimental data and calculated data [9, 10]. Several different models, such as noncentrosymmetric magnetic ordering [9] and acentric spin-density waves [11], were also proposed to explain the appearance of ferroelectricity in this kind of materials.

It has long been recognized that electron energy-loss spectra (EELS) in a transmission electron microscope (TEM) can provide rich information of the chemical bonding and local structures of materials [12]. EELS, as well as the equivalent technique X-ray absorption spectroscopy (XAS), is an important experimental technique detecting the unoccupied states of materials. Especially, the energy-loss near-edge structure (ELNES) which resolves electronic dipole transitions from the core states of a particular atom to unoccupied final states was found to be sensitive to variations of the chemical environment of a given element [12]. ELNES, along with the rapid development of electronic calculations, has been proved to be an efficient method to study the unoccupied band structure near Fermi energy and the correlation strength in certain functional oxides [13–15]. In the present work, we will report on the study of electronic structure of multiferroic YMn_2O_5 using GGA. The experimental oxygen K and manganese $L_{2,3}$ edge ELNES in YMn_2O_5 have been analyzed based on first-principles calculations. The

correlation effects have also been discussed for this kind of manganites.

2 Theoretical approach and experimental methods

The crystal structures of $REMn_2O_5$ used in our calculations are taken from the neutron powder diffraction data [7, 16]. $REMn_2O_5$ compounds have the $DyMn_2O_5$ type orthorhombic structure with a space group of *Pbam*, and each unit cell contains four formula units (f. u.) consisting of $Mn^{4+}O_6$ octahedra and $Mn^{3+}O_5$ pyramids, as schematically shown in Fig. 1. The octahedra share edges and form ribbons parallel to the c axis direction. Adjacent ribbons are linked by pairs of corner-sharing pyramids. The lattice parameters are $a = 7.2639$ Å, $b = 8.4758$ Å, $c = 5.6673$ Å for YMn_2O_5 [16] and $a = 7.6823$ Å, $b = 8.7056$ Å, $c = 5.7214$ Å for $LaMn_2O_5$ [7]. The full potential linearized augmented-plane-wave+local orbital (APW+LO) were used as implemented in WIEN2k code [17], with generalized gradient approximation (GGA, Wu–Cohen 06 [18]) for the exchange-correlation function. Self-consistency was carried out on a 3×3×2 mesh containing 8 k-points in the irreducible Brillouin zone (IBZ) to reach a good convergence of energy and charge. $R_{mt}K_{max}$ was set to 8.0 to determine the basis size, and RMTs were used 2.39 a. u., 1.87 a. u., and 1.66 a. u., for Y (La), Mn, and O, respectively. For the Mn-3d orbitals, an effective U obtained by a self-interaction correction (SIC) [19] is employed to study the electronic correlation effects on the electronic structure. The electron energy-loss near-edge structure (ELNES) was calculated using TELNES2.0 program implemented in the WIEN2k code [20, 21].

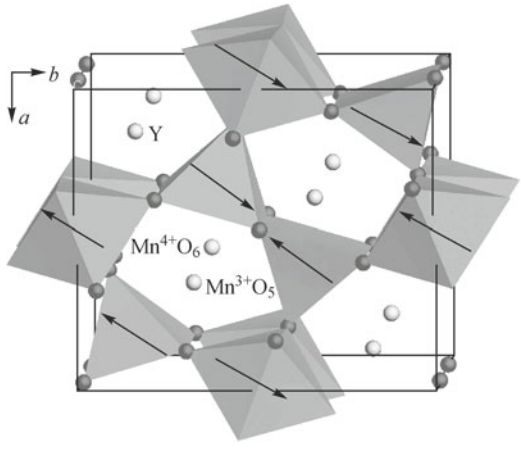

Fig. 1 Schematic structure of YMn_2O_5. The arrows denote the spin configuaration in our calculations. The octahedra and pyramids are schematically shown in the unit cell.

The experimental EELS measurements were carried out on an FEI Tecnai-F20 (200 kV) TEM equipped with a Gatan imaging filter (GIF). The energy resolution is about 1.0 eV as the full width at half-maximum (FWHM) of the zero loss peak collected without specimen. Single crystals of YMn_2O_5 were grown using $B_2O_3/PbO/PbF_2$ flux in a Pt crucible, as described in Ref. [8]. TEM samples were prepared by crushing the samples and dispersing the suspensions on a carbon-covered Cu grid.

3 Results and discussion

3.1 Electronic structure

We start our investigations of YMn_2O_5 for different types of spin configurations (SCs) in the ground-state. In previous literatures, it was pointed out that a collinear spin structure ignoring spin–orbit coupling could be a good approximation for this kind of materials [9, 10]. We therefore first performed our calculations on the total energies for different magnetic structures of para-(P), ferro-(F), and anti-ferro(AF)-magnetic states, respectively, the results suggest that AFM ground state, as illustrated in Fig. 1, has a lower energy of ∼113.3 meV/f. u. in comparison with the FM state in consistence with the experimental results [8]. Furthermore, we also used a 2×1×1 AFM supercell as discussed in Ref. [9] to carry out a detailed calculation, and similar results have been obtained. Figure 2(a) depicts the calculated DOS of YMn_2O_5 for the AFM state. Combined with the partial DOS in Fig. 3(a), it is clearly recognizable that the DOS between –7 eV and E_F is mainly governed by Mn-3d and O-2p orbital states, strong hybridization of Mn-3d and O-2p bonding commonly existent in this region. A careful analysis also demonstrates that the occupied Y-4d states lie in the same range as the O-2p states, and the unoccupied Y-4d states lie mainly in the energy range of 4–10eV above the Fermi level.

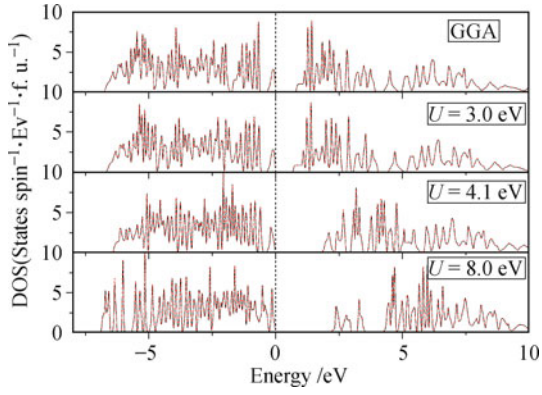

Fig. 2 DOS of YMn_2O_5 for **(a)** GGA, **(b)** $U = 3.0$ eV, **(c)** $U = 4.1$ eV, **(d)** $U = 8.0$ eV. Fermi energy is shifted to $E = 0$ eV. Spin up states are shown as black lines, while spin down states are shown as red dotted lines.

The energy gap as estimated in our calculation is about 0.8 eV for YMn_2O_5, which is larger than that obtained

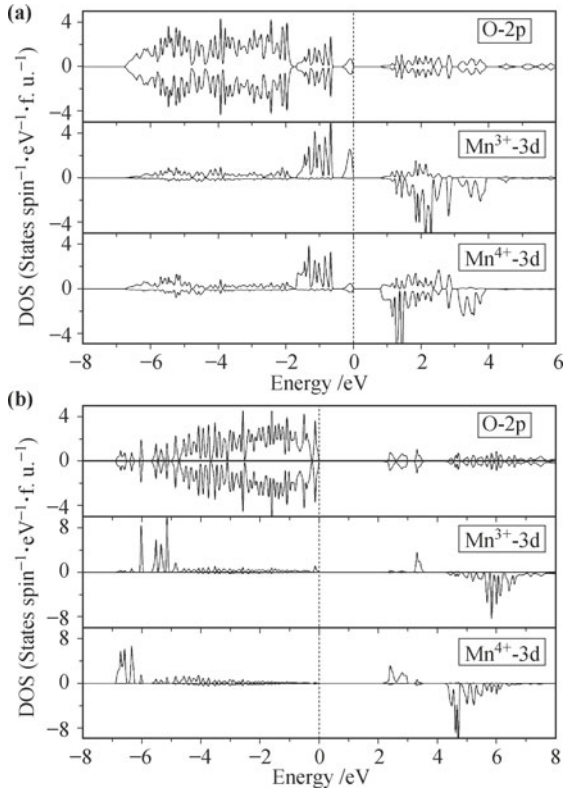

Fig. 3 O-2p and Mn-3d partial DOS of YMn_2O_5. **(a)** GGA; **(b)** $U = 8.0$ eV.

for $TbMn_2O_5$, i.e., ∼0.4 eV by using the psudopotential approach [10]. Previously, the optical property and the charge transfer gap have been measured in $TbMn_2O_5$ [22]. This gap corresponds mainly to the p–d charge transfer transitions as revealed in the spectral analysis of optical properties. In order to make a better measurement of the energy gap in YMn_2O_5, we carried out the experimental studies using the low energy loss spectrum in TEM at room temperature. It is commonly noted in previous literatures that the zero-loss peak (ZLP) subtraction from the experimental data could largely affect the measured value of a band gap [23–25]. We herein use the deconvolution data from another separately recorded ZLP, a technique having been proved a much more accurate method to get band gap [24, 25]. The band gap of YMn_2O_5 is estimated to be about 2.4 eV. It should be mentioned that in general the GGA approach could underestimate the band gap as discussed in Ref [26]. As the bands above and below the gap are mainly governed by the Mn-3d and O-2p orbitals, the correlation effects of Mn-3d electrons may affect the gap size significantly, as will be discussed in the following context.

The local magnetic moments on the Mn ions obtained in our calculation have the values of about $\sim 3.19\mu_B$ for Mn^{3+} and $\sim 2.46\mu_B$ for Mn^{4+}, respectively. These data are in good agreement with the neutron diffraction data in the low-temperature phase as measured at $T = 2$ K, i.e., $\sim 3.54\mu_B$ for Mn^{3+} and $\sim 2.48\mu_B$ for Mn^{4+} [27]. Furthermore, the charge difference between Mn^{3+} and Mn^{4+} ions based on the DOS for majority spin is expected to be $0.38e$, suggesting the presence of notable charge disproportion in the present system. These results are fundamentally consistent with previous discussions about the mix-valence states on $Mn^{3+}O_5$ and $Mn^{4+}O_6$ octahedra [9, 22, 28].

3.2 GGA+U

In order to understand the correlation effects on the electronic structure in these compounds, we use the GGA+U regime to investigate the alternation of the band structure for U in the range of $0 < U \leqslant 8$ eV. Figure 2 shows the calculated DOSs for different U, illustrating obvious changes of electronic structure with an introduction of correlation effects. The electronic bands near Fermi energy (E_F) become visibly narrower with the increase of U. Moreover, the band gap increases considerably from 0.80 eV for $U = 0$ to 2.08 eV for $U = 8.0$ eV, as clearly illustrated in Table 1. In addition, we also used the parameter free semi-local potential, a newly invented modified Becke–Johnson local density approximation (MBJLDA) technique, to study the band gap [29, 30]. We obtained a theoretical data for an energy gap of 1.90 eV in YMn_2O_5. As reported in previous studies this method could give rise to a relatively accurate gap for sp-semiconductors and insulators [30]. However, it should be mentioned that the efficiency of MBJLDA in the correlated materials is still under debate [31].

Table 1 Calculated Energy gap of YMn_2O_5 and $LaMn_2O_5$ using GGA+U.

Calculated	Energy gap/eV	
U/eV	YMn_2O_5	$LaMn_2O_5$
0	0.80	0.94
3.0	1.56	1.54
4.1	1.75	1.90
8.0	2.08	1.97

Careful analyses of the partial DOS calculated via GGA [Fig. 3 (a)] suggest that the Mn-3d and O-2p orbitals are strongly hybridized, so a strong covalent character of Mn–O bonding is expected. Figures 3 (b)–(d) shows the partial DOS calculated for different U. While U increases, it is recognizable that the occupied states of Mn-3d orbitals shift progressively to lower energy and, on the other hand, the occupied O-2p states shift to higher energy. This fact could lead to a more ionic Mn–O bonding. The Mn-3d states for $U = 8.0$ eV are mainly located in $-7 \sim -5$ eV below E_F, demonstrating a dominantly ionic Mn–O bonding character in the strongly correlated state. Based on the EELS measurements, certain bonding features have been carefully discussed in the following context. According to our calculations that the magnetic moments of Mn^{3+} and Mn^{4+} are 3.19 μ_B, 2.46 μ_B for $U = 0$, 3.40 μ_B, 2.69 μ_B for $U = 3$ eV, 3.46 μ_B, 2.76

μ_B for $U = 4.1$ eV and 3.61 μ_B, 2.99 μ_B for $U = 8$ eV, respectively. The data with $U \leqslant 4.1$ eV are comparable with the experimental moments ($\sim$3.54 μ_B for Mn^{3+} and $\sim$2.48 μ_B for Mn^{4+}) [27].

3.3 Comparison between theoretical and experimental EELS

ELNES measurements can provide a rich variety of information about the electronic structure and the unoccupied states near E_F. In the present study, we have performed systematic measurements on YMn_2O_5 and compared with theoretical results. Figure 4 shows the experimental EELS of the oxygen K-edge after background subtraction and multiple scattering deconvolution for YMn_2O_5. Both the experimental data and theoretical results are displayed for comparison. All calculated spectra are broadened to match the experimental data with a resolution of about 1.0 eV.

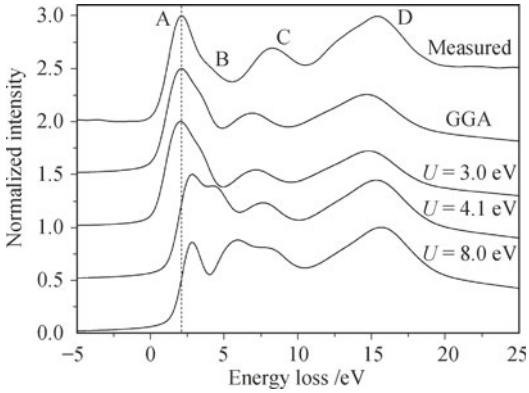

Fig. 4 Experimental and simulated O–K edge of YMn_2O_5. The dotted line refers to the peak A position of the measured spectrum as guide line. All spectra are aligned using the onset of experimental O–K edge. The Gaussian broadening for the simulated spectra is 1.0 eV.

The oxygen K-edge spectra are from O-1s to 2p transitions, showing notable features corresponding to the oxygen p-projected DOS of ground state. YMn_2O_5 is known as a typical ionic insulators in which the core hole potential has been considered to have limited effect on the structural features for the O–K edges [32, 33], so in the present study, we ignore the core-hole effects in our theoretical simulations. Actually, the GGA data could give rise to the O–K edges with very similar features in comparison with the experimental data. The peak positions from both theoretical and experimental data are listed in Table 2. In order to facilitate the analysis of spectral structures, all theoretical and experimental spectra have been aligned using the edge onset of experimental spectrum in Fig. 4, and the energy of all peaks are listed in Table 2. As is clearly indicated in Fig. 4, the four main peaks can be well interpreted based on our theoretical results. Peak A appearing at the position of 2.1 eV above Fermi level are the transitions from O-1s towards the unoccupied O-2p that have been hybridized by Mn-3d orbitals. A shoulder in the higher side of Peak A at the position of about 4 eV, labeled as Peak B, also arises from the O-2p and Mn-3d hybridized orbitals. Peak C, at the position of about 8.3 eV, is much broader in comparison with Peak A, which can be interpreted as the transitions of O-1s to the unoccupied states mixed by Y-4d, a small fraction of Mn-3d and O-2p orbitals. Peak D at the position of about 15.4 eV in general is very broad as also observed in other transition metal (TM) oxides [34]. This feature stems from the hybridization of the O-2p orbital with Mn-4sp and Y 5s orbitals.

Table 2 O–K edge peaks position. All spectra are aligned using the edge onset of the experimental spectrum. The peak B is estimated by the local maximum of the first differentiation of the spectra.

Calculated	Peaks/eV			
U/eV	A	B	C	D
0	2.10	3.20	6.91	14.66
3.0	2.04	3.11	7.16	14.80
4.1	2.83	4.24	7.64	15.32
8.0	2.83	5.92	7.77	15.65
Measured	2.1±0.1	4.0±0.1	8.3±0.1	15.4±0.1

The two peaks, A and B, both are attributed to transitions from O-1s core state to O-2p states hybridized with mixed valent Mn-3d orbitals. However, just as discussed for the compounds of $La_{1-x}A_xMnO_3$ (A = Ca, Sr), the exact assignment of these fine structural features in these peaks are still controversial in literatures [35]. A careful analysis of the electronic band structure by GGA shows that these peaks can be fundamentally interpreted in association with charge segregation on the Mn sites. According to the calculated partial DOS as shown in Fig. 3(a), the main peaks of Mn^{3+} and Mn^{4+} 3d states have a separation of $\sim$1 eV apart, which is in agreement with the energy separation of calculated spectra of the peaks A and B. So the peak split of the first peak of O–K edge originates mainly from the charge disproportion of Mn atoms through the Mn–O hybridization. In another word, Peak A is mainly from $Mn^{4+}O_6$, and Peak B is mainly from $Mn^{3+}O_5$, and no notable contribution of crystal field split is observed in this study [36]. This interpretation of these two peaks is also consistent with the understanding of the spectral structure of Mn-L_3 edge as shown in Fig. 5, which shows similar structural feature as obtained from the XAS measurement for $BiMn_2O_5$ [36].

It is noted that peak B in our simulated spectra (when $U < 4.1$ eV) lies at a slightly lower position compared with the experimental spectra. This discrepancy may result from the following factors. The site dependent chemical shift can be the predominant factor and the charge transfer effect between two Mn sites might also play an important role. It is worth noting that the energy

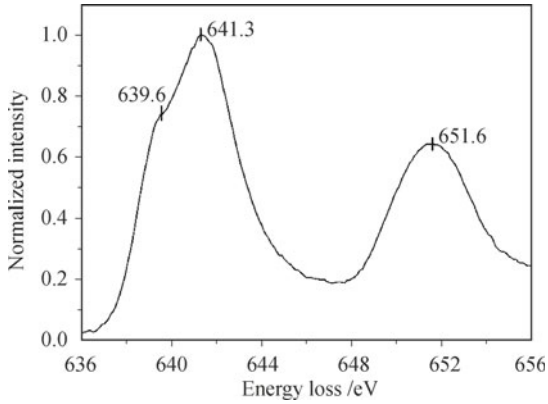

Fig. 5 Experimental Mn-$L_{2,3}$ edge. The edge of L_3 splits into two peaks separated by about 1.7±0.1 eV. The full-width at half-maximum (FWHM) of L_3 edge is ∼4.6±0.1 eV.

separations between all the four peaks in the simulated spectra are slightly smaller than those in the experimental ones, and peak separations A–C and C–D keep almost unchanged with the increase of U. Compared with the experimental data, the slight discrepancy of theoretical peak D is considered coming from the local structural distortion [12], and the relatively large discrepancy for peak C is believed to have resulted from the correlation effects of Y-4d orbitals. Actually, we have performed certain theoretical calculations with consideration of correlation effects, and the theoretical peak C could fundamentally coincide with the experimental one. To understand the fine structures of the EELS, a detailed analysis of the correlation effects on specific orbitals of Mn and Y is in progress. To unravel the correlation effects on the EELS data, we considered the theoretically simulated O–K edge for $0 < U \leqslant 8.0$ eV. It is noted that the calculated spectra for $U < 4.1$ eV can well reproduce all peaks appearing in the experimental spectra. Their positions, as well as relative intensities, agree well fundamentally with the experimental ones. The most striking feature in the theoretical O-K edge spectra is the appearance of the remarkable position and intensity change of peaks A and B, and so the peak width of the first two peaks increases when U is increased to 4.1 eV. While U is further increased to 8.0 eV, the position of peak B is further shifted to higher energy. These phenomena result from the evolution of band structures along with the increase of U. As we discussed above, as U rises, the conduction bands narrow down, Mn 3d and O 2p hybridization is weakened and Mn–O bonding becomes more ionic. In unoccupied states, the Mn-3d states are shifted from near E_F to higher energy. These partial DOS shifts directly lead to a larger band gap and a spectra weight shift of O–K edge (see peak B). In addition to the consideration of the gap size as discussed above, we therefore conclude that the on-site interaction U in YMn_2O_5 is less than 4 eV. In fact, the electron correlation U has also been discussed in another compound of $HoMn_2O_5$ [37] in understanding the ferroelectric polarization, in which U is estimated to be as large as 8 eV. In addition, our experimental measurements of the spectra of Mn-$L_{2,3}$ edges also reveal clear peak splits that can be contributed to the charge disproportions of Mn^{3+} and Mn^{4+}, respectively. However, theoretical simulation of the $L_{2,3}$ edge needs special consideration in terms of the multiplet effects [38], and a detailed analysis is still in progress.

As revealed in our theoretical study, $LaMn_2O_5$ has very similar electronic structure features comparable with those of YMn_2O_5 as illustrated in Figs. 2 and 6. The La substitution for Y could generate certain additional unoccupied La-4f orbital states in $LaMn_2O_5$; it appears at ∼4.5 eV above E_F. On the other hand, it is also recognized that the valence bands slightly below E_F of $LaMn_2O_5$ are narrower than that of YMn_2O_5. This variation is considered to have come from a relatively larger radius of the La ion, which may also lead to an increase of the band gap, as listed in Table 1.

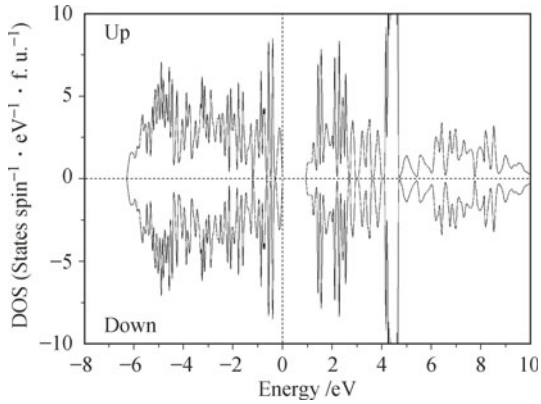

Fig. 6 DOS of $LaMn_2O_5$ calculated using GGA. Up and down denotes the DOS of spin up and spin down, respectively.

4 Conclusions

In summary, the electronic structures of YMn_2O_5 have been studied by use of GGA and GGA+U ($0 < U \leqslant 8$ eV). The strongly hybridized Mn-O bonding character has been demonstrated based on our careful analysis of the electronic band structure. The GGA+U calculations reveal that the presence of the on-site Coulomb interaction U could result in the increase of the band gap, but may weaken the Mn–O hybridization. A systematic analysis of the theoretical and experimental EELS for O–K edge suggests that the electronic correlation U in YMn_2O_5 could be less than about 4 eV. The certain electronic structural features of $LaMn_2O_5$ have been discussed in comparison with the data of YMn_2O_5.

Acknowledgements This work was supported by the National Natural Science Foundation of China (Grant Nos. 10874227, 90922001, 10874214, 11074292, and 10904166), the Knowledge Innovation Project of the Chinese Academy of Sciences, the National Basic Research Program of China (973 Program), and the National

High Technology Research and Development Program of the Ministry of Science and Technology of China (863 Program).

References

1. W. Eerenstein, N. D. Mathur, and J. F. Scott, Nature, 2006, 442: 759
2. G. Catalan and J. F. Scott, Adv. Mater. (Deerfield Beach Fla.), 2009, 21: 2463
3. N. Hur, S. Park, P. A. Sharma, J. S. Ahn, S. Guha, and S. W. Cheong, Nature, 2004, 429: 392
4. N. Hur, S. Park, P. A. Sharma, S. Guha, and S. W. Cheong, Phys. Rev. Lett., 2004, 93: 107207
5. C. R. dela Cruz, F. Yen, B. Lorenz, M. Gospodinov, C. Chu, W. Ratcliff, J. Lynn, S. Park, and S. W. Cheong, Phys. Rev. B, 2006, 73: 100406
6. P. G. Radaelli, L. C. Chapon, A. Daoud-Aladine, C. Vecchini, P. J. Brown, T. Chatterji, S. Park, and S. W. Cheong, Phys. Rev. Lett., 2008, 101: 067205
7. A. Munoz, J. A. Alonso, M. T. Casais, M. J. Martinez-Lope, J. L. Martinez, and M. T. Fernandez-Diaz, Eur. J. Inorg. Chem., 2005, 2005: 685
8. C. Vecchini, L. Chapon, P. Brown, T. Chatterji, S. Park, S. W. Cheong, and P. Radaelli, Phys. Rev. B, 2008, 77: 134434
9. C. Wang, G. C. Guo, and L. He, Phys. Rev. Lett., 2007, 99: 177202
10. C. Wang, G. C. Guo, and L. He, Phys. Rev. B, 2008, 77: 134113
11. L. C. Chapon, P. G. Radaelli, G. R. Blake, S. Park, and S. W. Cheong, Phys. Rev. Lett., 2006, 96: 097601
12. R. Egerton, Electron Energy-Loss Spectroscopy in the Electron Microscope, New York and London: Plenum Press, 1996
13. S. L. Dudarev, G. A. Botton, S. Y. Savrasov, Z. Szotek, W. M. Temmerman, and A. P. Sutton, Phys. Status Solidi (a), 1998, 166(1): 429
14. R. Xiao, H. Yang, L. Xu, H. Zhang, Y. Shi, and J. Li, Solid State Commun., 2005, 135(11–12): 687
15. G. Radtke, A. Saúl, H. Dabkowska, B. Gaulin, and G. Botton, Phys. Rev. B, 2008, 77: 125130
16. C. Delacalle, J. Alonso, M. Martinezlope, M. Garciahernandez, and G. Andre, Mater. Res. Bull., 2008, 43(2): 197
17. P. Blaha, K. Schwarz, G. K. H. Madsen, D. Kvasnicka, and J. Luitz, Karlheinz Schwarz, Techn. University Wien, Austria, 2001
18. Z. Wu and R. E. Cohen, Phys. Rev. B, 2006, 73: 235116
19. V. I. Anisimov, I. V. Solovyev, M. A. Korotin, M. T. Czyzyk, and G. A. Sawatzky, Phys. Rev. B, 1993, 48: 16929
20. M. Nelhiebel, P. H. Louf, P. Schattschneider, P. Blaha, K. Schwarz, and B. Jouffrey, Phys. Rev. B, 1999, 59: 12807
21. J. Titantah, K. Jorissen, and D. Lamoen, Phys. Rev. B, 2004, 69: 125406
22. A. Moskvin and R. Pisarev, Phys. Rev. B, 2008, 77: 060102
23. B. Rafferty and L. M. Brown, Phys. Rev. B, 1998, 58: 10326
24. B. Rafferty, S. J. Pennycook, and L. M. Brown, J. Electron Microsc. (Tokyo), 2000, 49(4): 517
25. M. Stöger-Pollach, Micron, 2008, 39(8): 1092
26. J. Heyd, J. E. Peralta, G. E. Scuseria, and R. L. Martin, J. Chem. Phys., 2005, 123: 174101
27. P. G. Radaelli, C. Vecchini, L. C. Chapon, P. J. Brown, S. Park, and S. W. Cheong, Phys. Rev. B, 2009, 79: 020404
28. J. Koo, C. Song, S. Ji, J. S. Lee, J. Park, T. H. Jang, C. H. Yang, J. H. Park, Y. H. Jeong, K. B. Lee, T. Y. Koo, Y. J. Park, J. Y. Kim, D. Wermeille, A. I. Goldman, G. Srajer, S. Park, and S. W. Cheong, Phys. Rev. Lett., 2007, 99: 197601
29. A. D. Becke and E. R. Johnson, J. Chem. Phys., 2006, 124: 221101
30. F. Tran and P. Blaha, Phys. Rev. Lett., 2009, 102: 226401
31. D. J. Singh, Phys. Rev. B, 2010, 82: 205102
32. P. Rez and D. A. Muller, Annu. Rev. Mater. Res., 2008, 38(1): 535
33. J. B. Neaton, D. A. Muller, and N. W. Ashcroft, Phys. Rev. Lett., 2000, 85: 1298
34. F. M. F. De Groot, M. Grioni, J. C. Fuggle, J. Ghijsen, G. A. Sawatzky, and H. Petersen, Phys. Rev. B, 1989, 40: 5715
35. N. Mannella, A. Rosenhahn, M. Watanabe, B. Sell, A. Nambu, S. Ritchey, E. Arenholz, A. Young, Y. Tomioka, and C. S. Fadley, Phys. Rev. B, 2005, 71: 125117
36. D. K. Shukla, S. Mollah, R. Kumar, P. Thakur, K. H. Chae, W. K. Choi, and A. Banerjee, J. Appl. Phys., 2008, 104: 033707
37. G. Giovannetti and J. van den Brink, Phys. Rev. Lett., 2008, 100: 227603
38. F. Groot, Coord. Chem. Rev., 2005, 249(1–2): 31